



Study on electroelastic field concentration around the electrode tip in multilayer ferroelectric actuators of two designs and their optimizations

X.J. Zhao, B. Liu ^{*}, D.N. Fang ^{*}

AML, Department of Engineering Mechanics, Tsinghua University, Beijing 10084, China

ARTICLE INFO

Article history:

Received 31 May 2009

Received in final revised form 30 August 2009

Available online 19 September 2009

Keywords:

Piezoelectric/ferroelectric actuator

Electrode

Electromechanical concentration

Finite element method

Optimization

ABSTRACT

Distribution of electromechanical field near electrode tips is closely related to the reliability of ferroelectric multilayer actuators. In this paper, the deformation and stress concentrations around the electrode tip in two multilayer actuator designs, partially and fully cofired, are investigated by means of experimental measurement and numerical simulations. The digital speckle correlation method (DSCM) is used to measure the full displacement field near the electrode tip with the high spatial resolution. The paths of electric breakdown and cracks initiated from the edge of electrodes were observed. With the proposed Double Gibbs free energy criterion, a fully coupled nonlinear electromechanical finite element method based on domain-switching mechanisms is developed and the simulation results agree well with the experiments. It is found that the crack-like “defects” in the partially cofired layered actuators, i.e. the interlayer gaps filled with soft insulating wax, can significantly reduce the maximum tensile stress level compared with that in “perfect” fully cofired actuators, which implies that the partially cofired design is more reliable than the fully cofired one. Further optimization on geometrical dimension of actuators is also carried out.

© 2009 Elsevier Ltd. All rights reserved.

1. Introduction

Multilayer piezoelectric actuators have been widely employed in the fields of high-precision positioners, motors and vibration suppressors because of their precise microscopic displacement, large generative force and quick response (Uchino and Takahashi, 1996). A typical multilayer actuator often consists of hundreds of ceramic layers, alternating with internal electrodes. The electric field near terminated electrode edges is non-uniform and much higher than that elsewhere in the ferroelectrics (Gong and Suo, 1996). The strain incompatibility induced by the non-uniform electric field near the electrode tip could result in a highly complex and concentrated stress field, which may cause the crack initiation and propagation from the vicinity of electrode edges, and finally lead to the failure of the devices. Generally, most piezoelectric actuators are made of ferroelectric ceramics which show strong nonlinear behaviors due to the domain-switching caused by the high electric field concentration. Therefore, it is difficult, but of great practical significance to predict the concentrated electromechanical fields at the electrode tip.

Research efforts have been made to investigate the destruction mechanism associated with the interaction between the electrodes and piezoelectric materials. Experimental observations suggest that the cracks are prone to arise in the region near the edge of electrodes (Furuta and Uchino, 1993; Aburatani et al., 1994; Liu et al., 2002, 2005). For electrostrictive ceramics containing internal electrodes, a number of models were developed to study the electromechanical field

^{*} Corresponding authors. Tel.: +86 10 62786194; fax: +86 10 62781824 (B. Liu).

E-mail addresses: liubin@tsinghua.edu.cn (B. Liu), fangdn@mail.tsinghua.edu.cn (D.N. Fang).

concentrations near the electrodes due to the quadratic electrostriction (Winzer, 1989; Hom and Shankar, 1995; Yang and Suo, 1994; Hao et al., 1996; Gong and Suo, 1996). There are also some theoretical models developed to analyze the stress singularity in piezoelectric materials caused by electrodes based on the linear piezoelectric theory (Ru, 2000; Liu et al., 2000; Ye and He, 2001; Li and Tang, 2003; Narita et al., 2004; Wang, 2005). Guo et al. (2006) presented a linear electromechanical meshless method based on moving least square interpolation and conducted a numerical analysis for the multilayered piezoelectric actuator containing internal electrodes.

To quantify the effect of the interaction between electrodes and piezoelectrics, experimental approach is an essential way to validate the analytical and numerical models. Recently, the deformations near the electrode tip were measured with morié interferometry technique and strain gages, respectively, and the finite element (FE) simulations were then carried out to simulate the electrode-induced field concentration (Qiu et al., 2004; Yoshida et al., 2003; Shindo et al., 2004). However, the morié interferometry technique can only provide limited pattern information in the small region near the electrode tip. On the other hand, the strains obtained from strain gages, in fact, are average values in the local areas due to the large coverage of gages compared to the thickness of ceramic layers, which may not be able to precisely measure the deformation near the electrode tip. Actually, Shindo et al.'s results (2004) show that the disagreement between the computation and strain gage measurement tends to be significant when close to the electrode tip. Following Shindo et al.'s experiment, Elhadrouz et al. (2006) developed a nonlinear FEM based on a simplified phenomenological constitutive law to investigate the electroelastic concentration ahead of electrode tip for a multilayer ferroelectric actuator.

In spite of the existing work on piezoelectrics with electrodes mentioned above, distributions of electroelastic fields and the fracture mechanism caused by electrodes are still unclear, especially lack of accurate experimental data. On the other hand, the previous FEM simulations mostly focus on the modeling of linear piezoelectric systems, or they are only first-order approximations of nonlinear electromechanical field for ferroelectrics in which the domain distribution and the electromechanical field are not fully coupled and the former only depends on the latter.

In this paper, both experimental and numerical studies on electroelastic field concentrations near the electrodes in ferroelectrics are presented. The full-field deformation in the neighborhood of electrode tip under electric loading is quantitatively measured via Digital Speckle Correlation Method (DSCM) and optical microscopy. The paths of electrical breakdown and crack initiated at the edge of electrodes are in situ observed visually. A fully coupled nonlinear electromechanical FEM based on the domain-switching mechanism is then developed to simulate the electroelastic field concentrations, in which a new Double Gibbs free energy criterion is proposed to predict the evolution of domain distribution. The simulation results show a good agreement with the experiment. Moreover, the geometrical dimension of electrodes is optimized based on the nonlinear FEM analysis.

The present paper is structured in the following way. The experimental study on the electroelastic field in the neighborhood of electrode tip for the partially cofired actuator is presented in Section 2. A fully coupled nonlinear finite element method is proposed in Section 3, together with a numerical analysis on the partially cofired layered actuator. The electroelastic fields in both the partially cofired design and the fully cofired design are compared in Section 4, and the geometrical dimension optimization is performed and discussed in Section 5.

2. Experimental study on the electromechanical field near the electrodes of the partially cofired layered actuator

There are two types of designs for the multilayer actuators depending on the different cofiring area between the neighboring layers. Fig. 1a shows a fully cofired design scheme of a layered actuator, in which the piezoelectric layers, including the tab areas ahead of electrodes, are perfectly cofired together. Fig. 1b schematically shows a partially cofired design of layered piezoelectric actuators. Rather than assemble the piezoelectric ceramics layers as an integrated bulk, the actuator is just cofired partially and consists of interfacial gaps ahead of electrodes. For the partially cofired design, most part of the ferroelectric layer is covered by electrodes, and the rest ahead of electrode tip is separated by a very thin wax layer for the purpose of insulation (denoted by yellow segments in Fig. 1b), which is too soft to provide the interlayer adhesive stress. Therefore, from the mechanical point of view, the interfacial gap ahead of electrode tip is equivalent to a crack with free surfaces. However, from the corresponding electrical point of view, the electrode behaves like an electric "crack", and the insulating layer does not affect the distribution of electric field in the piezoelectrics since the layer is very thin and the wax/ceramic interface is parallel to the electric field. We note with interest that these two designs provide two combinations of mechanical and electrical discontinuities along or in the front of the electrodes, respectively. Therefore, it is worth studying the concentrated electroelastic fields near the electrode tip in both the fully and partially cofired designs. Since previous investigations mainly focused on the fully cofired layered actuators, in this paper the partially cofired one is studied and then compared with the fully cofired design.

The specimen used in the experiment is an eight-layer model actuator with internal electrodes, as shown in Fig. 2. This model actuator is built up with alternating electrodes and soft lead zirconate titanate (PZT) ferroelectrics layers by means of the tape-casting method. The practical and schematic pictures of the device are shown in Fig. 2a and b. The thickness of ceramic layers is 2 mm, which is much larger than the practical actuators. It should be pointed out that this magnified configuration is just a testing model that is fabricated by the same manufacturing process as the commercial one, but it can provide much more convenience for experimental measurement. After the assembly, the model actuator is poled under high electric field in silicon oil bath.

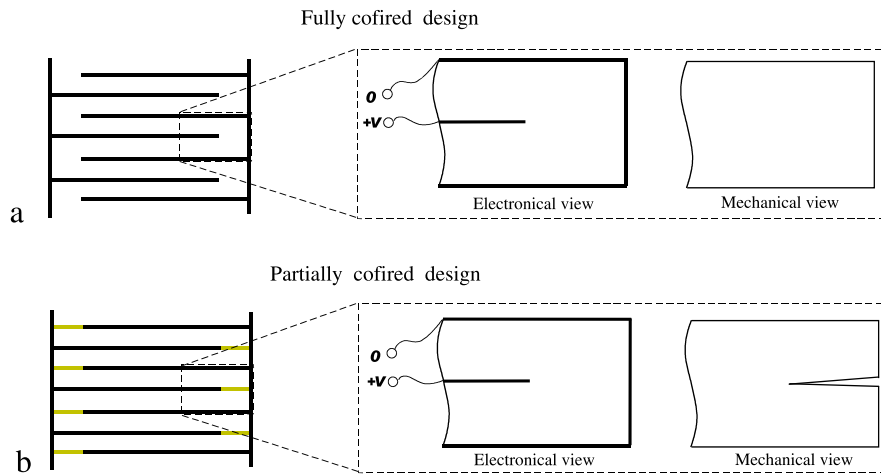


Fig. 1. Schematics of two designs on multilayer piezoelectric actuators and their equivalent zoom in views: (a) fully cofired design, (b) partially cofired design (yellow segments denote insulated wax) (For interpretation of the references to colour in this figure legend, the reader is referred to the web version of this article.).

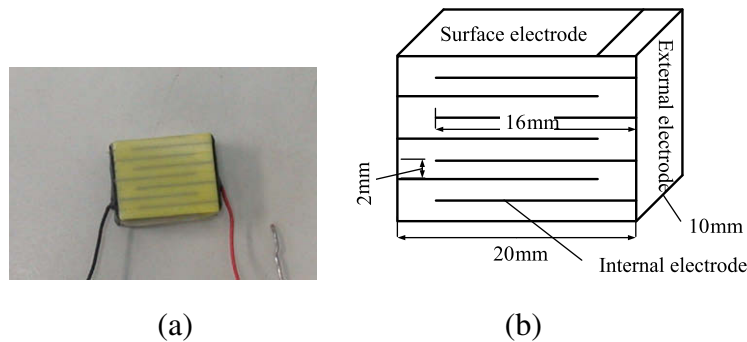


Fig. 2. The specimen (a) and its schematic diagram (b).

Although the large strain arises in the local area near the electrode tip, the displacement of piezoelectric materials under electric field is quite small and difficult to measure. The emergence of new optical techniques, such as Digital Speckle Correlation Method (DSCM) developed by Peters and Ranson (1982), has brought new opportunities in the microscale experimental mechanics. DSCM has a high spatial resolution, generally 0.01–0.05 pixel, and even can obtain the displacement at the nanoscale when assisted with optical microscopes (Xie et al., 2004; Zhang et al., 2006) or electrical microscopes (Sabatè et al., 2006). Therefore, in our experiment, a DSCM system was set up to measure the displacement field near an electrode tip. The microscopic imaging system used in our experiments was comprised of an OLYMPUS BX60 optical microscope and a CCD camera. To make the image correlation possible, the faces of the actuators were polished. The specimen was placed in an insulating box, which was fixed to the object stage under the optical lens. The images with a magnification of 200 \times under different electric loads were obtained with the resolution of 768 \times 576 pixels and shown in Fig. 3. The horizontal silvery white strip is the internal electrode and the dark segment ahead of electrode tip is interlayer gap. The image system is calibrated with optical gratings and the spatial resolution is obtained as 1.2050 $\mu\text{m}/\text{pixel}$ under the 200 \times magnification. Due to the symmetry of structure, only the image in the rectangle box (see Fig. 3), as small as 626.6 \times 253.0 μm , is selected as the correlation area for DSCM. Then the full displacement field near the electrode edge can be obtained by the correlation analysis of images.

Fig. 4 shows the corresponding contour lines of the y-direction displacement under the electric field of $E = 900 \text{ V}/\text{mm}$. The electrode tip is set as the origin of the coordinate system. It can be seen that the actuator elongates along the vertical direction on the whole, but the deformation field is intensely non-uniform and highly concentrated in the small region near the electrode tip, where the stress concentrations are speculated. But these concentrations diminish gradually with the departure from the electrode tip. It is also found that the interface gap ahead of the electrode tip opens when subjected to external electric field, which implies that the interface gap in the partially cofired actuator behaves like a mechanical crack due to the weak constraint of soft wax layer.

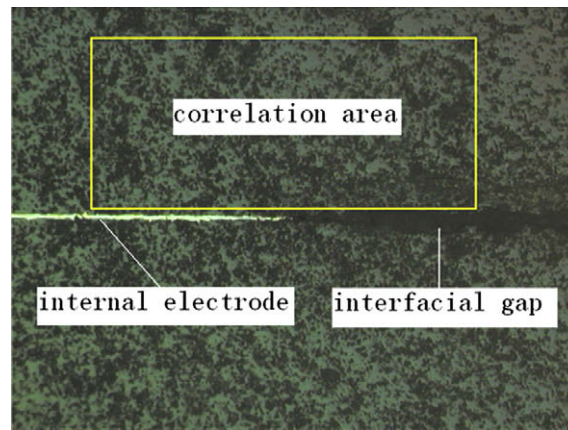


Fig. 3. Speckle image under the optical microscope at 200 \times magnification.

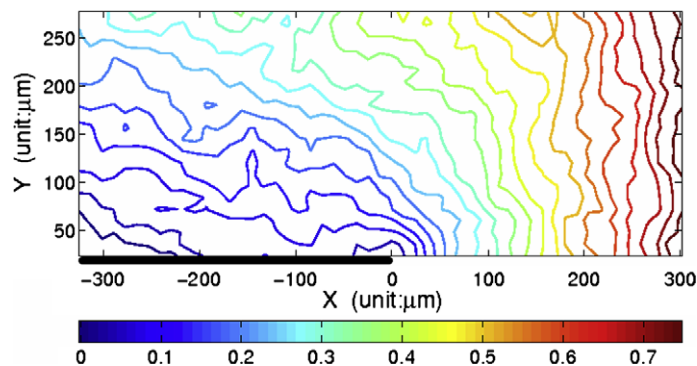


Fig. 4. Experimental y-direction displacement field of the partially cofired design (unit: μm).

With the increase of the electric field, the electrical breakdown and cracks are initiated from the local zone near the electrode edge. Figs. 5 and 6 show the paths of electrical breakdown and cracks near the electrode tip observed via optical microscope. As it can be seen, the dielectric surface breakdown tends to discharge obliquely from the electrode tip to the paired electrode, which indicates that the largest electric field may occur in this direction and make the electrical breakdown possible. However, it is interesting that cracks propagate preferentially along the ceramic–electrode interfaces. We suppose that the interface fracture may be caused by the strong tensile stress around the electrode edges. Considering that the stress can not be measured directly in experiments due to the electromechanical coupling, we will further investigate this guess in the ensuing finite element analysis.

3. Fully coupled nonlinear finite element analysis of the electroelastic field near the electrodes of the partially cofired layered actuator

3.1. Fully coupled nonlinear finite element method

Finite element method is a promising tool to probe complicated electromechanical phenomena. Several efforts have been made to deal with the computation of macroscopic responses based on microscopic model, in which the macroscopic remanent polarization and strain can be obtained by volume average over all crystallites of the local values. By assuming that the crystal consists of many domains and the domain can switch by a discrete angle when an energetic criterion is met, the constitutive behavior of ferroelectrics can be implemented by electromechanical finite element method (Chen and Lynch, 1999; Hwang and McMeeking, 1999; Kamlah et al., 2005). On the other hand, a good many of computational models have been developed based on the phenomenological constitutive laws, which is simple to be implemented in an FE-code with realistic effort (Kamlah and Tsakmakis, 1999; McMeeking and Landis, 2002; Su and Landis, 2007; Liu et al., 2008).

In the present paper, a two-dimensional plain strain nonlinear FEM incorporating the three-dimensional constitutive model is devised to model the evolution of domain structures in ferroelectrics and electromechanical behaviors around the electrode tip. The displacement u and the electric potential ϕ are chosen as basic field variables. The Einstein summation

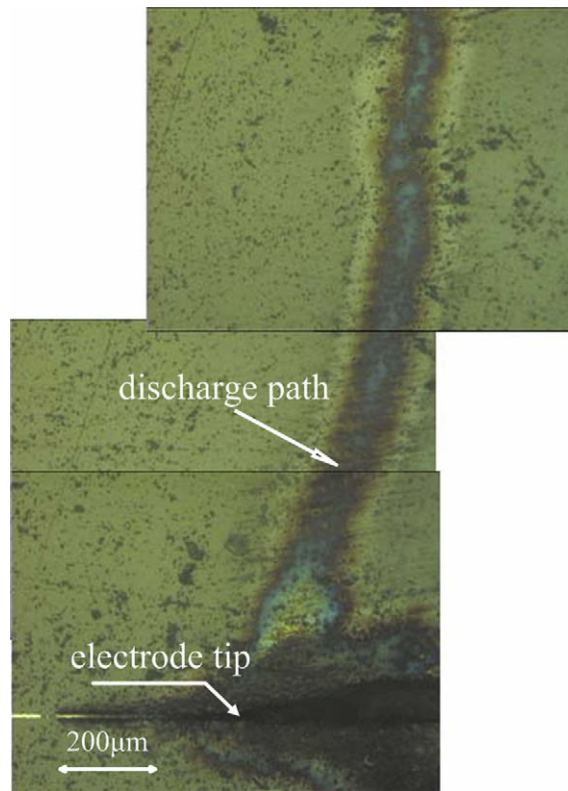


Fig. 5. Path of electrical breakdown near the electrode tip.

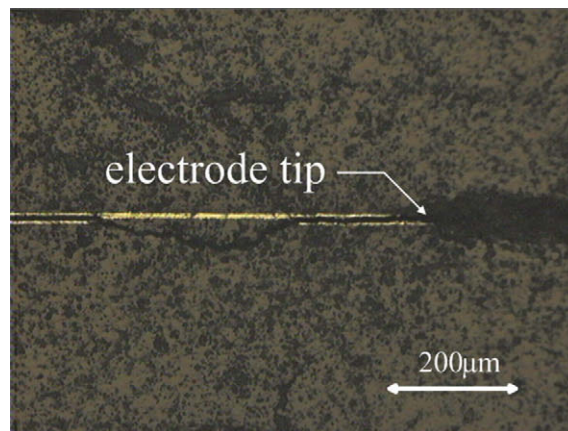


Fig. 6. Cracking patterns near the electrode tip.

convention over repeated indices is used for convenience and the comma denotes partial differentiation with respect to the coordinate x_i . The governing equations are listed as follows.

Generalized kinematics equations:

$$\varepsilon_{ij} = \frac{1}{2}(u_{i,j} + u_{j,i}) \quad (1)$$

$$E_i = -\frac{\partial \phi}{\partial x_i} \quad (2)$$

where ε_{ij} are the strain and E_i represent the electric field.

Generalized equilibrium equations:

$$\sigma_{ij,i} + f_j = 0 \quad (3)$$

$$D_{i,i} = p^e \quad (4)$$

where σ_{ij} , f_j , D_i and p^e are the stress, body force, electric displacement and electric volume charge, respectively.

Constitutive equations:

$$\sigma_{ij} = C_{ijmn}^E (\varepsilon_{mn} - \varepsilon_{mn}^*) - e_{nij} E_n \quad (5)$$

$$D_i = e_{imn} (\varepsilon_{mn} - \varepsilon_{mn}^*) + k_{in}^E E_n + D_i^* \quad (6)$$

where C_{ijmn}^E , e_{nij} and k_{in}^E are stiffness modulus, piezoelectric modulus and dielectric modulus, respectively (the superscript ε in k_{in}^E represents that these quantities are obtained under constant strain condition). ε_{mn}^* is the remanent strain and D_i^* is the remanent electric displacement. It should be noted that C_{ijmn}^E , e_{nij} , k_{in}^E , ε_{mn}^* and D_i^* will change with coordinates x_i and can be completely determined from the domain distribution at that material point. For simplicity, the material is modeled as isotropic elastic and isotropic dielectric.

The boundary conditions are

$$\begin{aligned} \sigma_{ij} n_i &= \bar{T}_j, \text{ on the given force boundary } S^\sigma, \\ D_i n_i &= \bar{p}^e, \text{ on the given charge boundary } S^D, \\ u_i &= \bar{u}_i, \text{ on the given displacement boundary } S^u, \\ \phi &= \bar{\phi}, \text{ on the given electric potential boundary } S^\phi, \end{aligned}$$

where \bar{T}_j and \bar{p}^e represent the applied surface force and surface charge, respectively. n_i denotes the outward normal vector, \bar{u}_i and $\bar{\phi}$ are prescribed displacement and electric potential, respectively.

Based on the assumption of continuum mechanics, we consider that each material point composes of many domains, and the dielectric and mechanical quantities of this point can be determined by averaging these domains. In our FEM simulation, linear triangle elements are used such that the properties of material are constants within each element and there is only one representative material point in this element. For each material point/element, 42 representative domains uniformly distributed in the orientation are chosen to model the behaviors of polycrystalline ferroelectrics. More details about the relation between domains and elements are given in Appendix A. If we know the domain distributions at any moment, all the material constants can be determined by volume averaging, and then the electromechanical field can be obtained via the electro-mechanical finite element method by solving the governing Eqs. (1)–(6) together with corresponding boundary conditions.

The nonlinear behavior of ferroelectric materials is primarily caused by domain-switching, so the proper domain-switching criterion plays a key role in the simulation of constitutive laws of ferroelectrics. By revising Hwang et al.'s (1995) criterion of domain-switching, Lu et al. (1999) proposed a Gibbs free energy criterion. The Gibbs free energy (per unit volume) in a domain can be expressed as

$$g(\sigma, \mathbf{E}, \mathbf{S}) = - \left(\boldsymbol{\varepsilon}^{(S)} : \sigma + \mathbf{D}^{*(S)} \cdot \mathbf{E} + \frac{1}{2} \sigma : \mathbf{M}^{E(S)} : \sigma + \frac{1}{2} \mathbf{E} \cdot \mathbf{k}^{\sigma(S)} \cdot \mathbf{E} + \mathbf{E} \cdot \mathbf{d}^{(S)} : \sigma \right) \quad (7)$$

where S denotes the domain type of the variables ($S = 1, 2, \dots, 6$), which is defined by Lu et al. (1999). Under the specific loading \mathbf{E} and σ , domain with different type S would have different Gibbs free energy g . In their original theory, the stress and the electric field change during the domain-switching process is not taken into account. Therefore, the Gibbs free energy in Eq. (7) is essentially $g(\sigma_{before}, \mathbf{E}_{before}, \mathbf{S})$, here σ_{before} and \mathbf{E}_{before} are the stress and electric field before domain-switching, and the driving force of switching is $g(\sigma_{before}, \mathbf{E}_{before}, \mathbf{S}_{before}) - g(\sigma_{before}, \mathbf{E}_{before}, \mathbf{S}_{after})$. \mathbf{S}_{before} and \mathbf{S}_{after} are domain types before and after switching. According to their theory, domains tend to switch to reach the new distribution with the minimum Gibbs free energy under the constant stress and electric field. When the driving force is larger than the threshold value of energy W^f , the domain-switching will take place.

It should be pointed out that the Gibbs free energy is only accurate in the case that the stress and the electric field keep constant during the domain-switching process. In fact, the stress and the electric field of a domain will most likely change when the domain-switching occurs, because a domain in a structure is usually constrained by other surrounding ones. Simply adopting the Gibbs free energy criterion will cause the domains to switch over more easily, and some switched domains will switch back to the original status if the Gibbs free energy criterion is still used after switching, which will make the iteration oscillatory and divergent. Therefore, this criterion is not appropriate in determining the domain-switching in a structure. Hence we propose a new criterion in this paper, which inherits the simplicity of the Gibbs free energy criterion but is applicable to more general situations. Specifically, not only the Gibbs free energies calculated from the stress and the electric field before switching, but also those after switching are considered, and only the domains satisfying both Gibbs free energy criteria (before and after switching) are allowed to switch. In other words, domain-switching from \mathbf{S}_{before} to \mathbf{S}_{after} is allowed only when $g(\sigma_{before}, \mathbf{E}_{before}, \mathbf{S}_{before}) - g(\sigma_{before}, \mathbf{E}_{before}, \mathbf{S}_{after}) \geq W^f$ and $g(\sigma_{after}, \mathbf{E}_{after}, \mathbf{S}_{before}) - g(\sigma_{after}, \mathbf{E}_{after}, \mathbf{S}_{after}) \geq W^f$, where σ_{after} and \mathbf{E}_{after} are the stress and electric field after domain-switching. We call this new criterion Double Gibbs free energy criterion (D-Gibbs criterion).

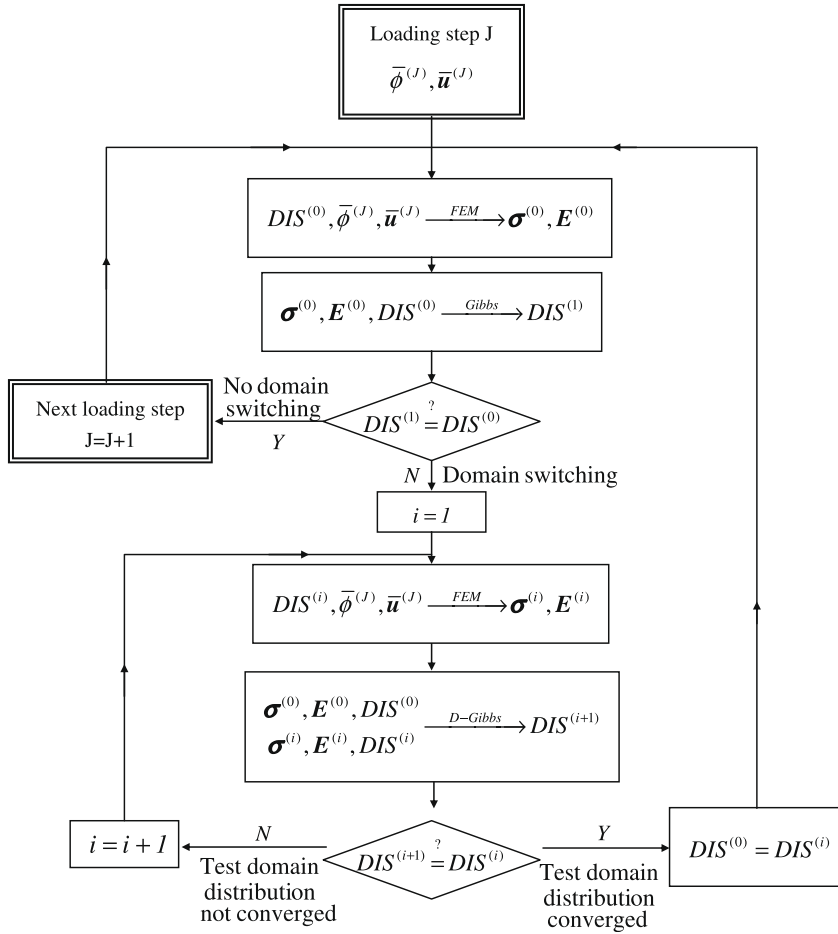


Fig. 7. FEM program flowchart.

However, we do not know the stress/electric field and the domain distribution after domain-switching, so we have to resort to iteration algorithm to solve it. In the program, we use the array DIS to record the domain distribution at each loading step, for example, $DIS^{(0)}$ is the domain distribution before switching. To find a reasonable domain distribution after switching, we first assign a guessed distribution after switching as $DIS^{(1)}$. Actually, in the program, we obtain it by using Gibbs free energy criterion (Lu et al., 1999). Then according to our D-Gibbs criterion, we can determine which domain-switching from $DIS^{(0)}$ to $DIS^{(1)}$ is allowable, and which is forbidden, so $DIS^{(1)}$ is revised to obtain a new distribution $DIS^{(2)}$. Next we apply the D-Gibbs criterion to $DIS^{(0)}$ and $DIS^{(2)}$ to determine $DIS^{(3)}$, and repeat the process until $DIS^{(i+1)} = DIS^{(i)}$. If each domain-switching from $DIS^{(0)}$ to $DIS^{(i)}$ is allowable according to D-Gibbs criterion, $DIS^{(i)}$ is then a reasonable distribution and we update $DIS^{(0)}$ with $DIS^{(i)}$. For each loading step, we repeat using this scheme to search reasonable domain-switching such that we can obtain the evolution of the domain distribution at each loading step. The program flowchart is presented in Fig. 7.

To demonstrate the validity of the proposed FEM with the new Double Gibbs energy criterion, the constitutive curves of ferroelectrics are computed. Fig. 8a and b show the polarization and butterfly hysteresis loops. The dash lines in these figures denote the experimental results by Hwang et al. (1995) and the solid lines are simulation results from our FEM. The material constants are chosen here to represent 8/65/35 PLZT. In this simple example, since the electric field and the stress are constants during the domain-switching process, the computational results are identical for Double Gibbs energy criterion and Gibbs energy criterion. We noted that our simulation can reasonably agree with the experimental results. Moreover, the time consumption is comparatively small, which makes it possible for large-scale computation.

3.2. Simulation model

Owing to the periodicity and the symmetry of structures (Fig. 9a), only half of an individual layer is simulated, as shown in Fig. 9b. The origin of the x - y coordinate system is placed at the electrode tip. The boundary conditions are listed as follows.

At the bottom electrode ($-L \leq x \leq 0, y = 0$),

$$\phi(x, 0) = V_{app}, \quad \tau_{xy} = 0, \quad u_y(x, 0) = 0 \tag{8a-c}$$

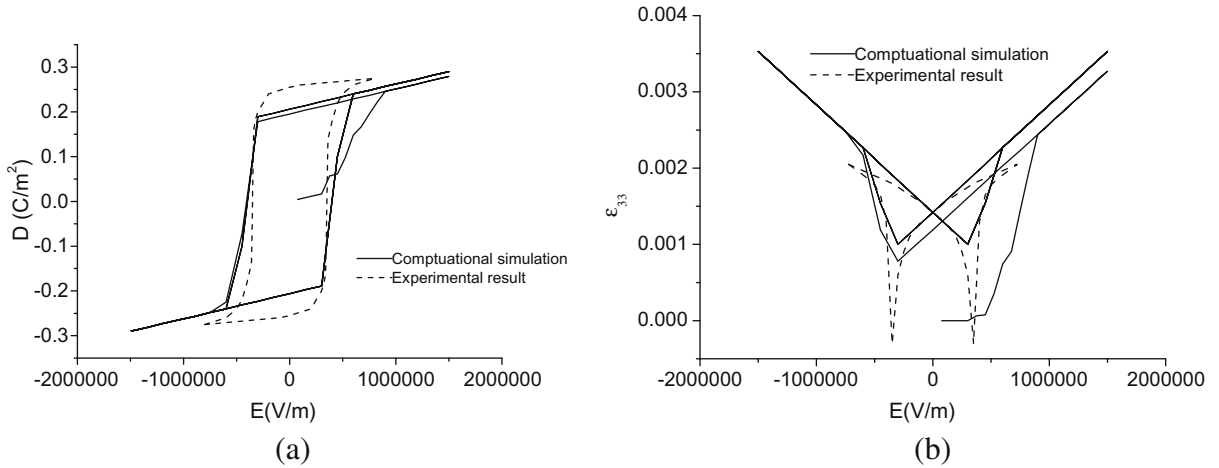


Fig. 8. (a) The variation of the electric displacement as the function of the electric field; (b) the variation of the strain as the function of the electric field.

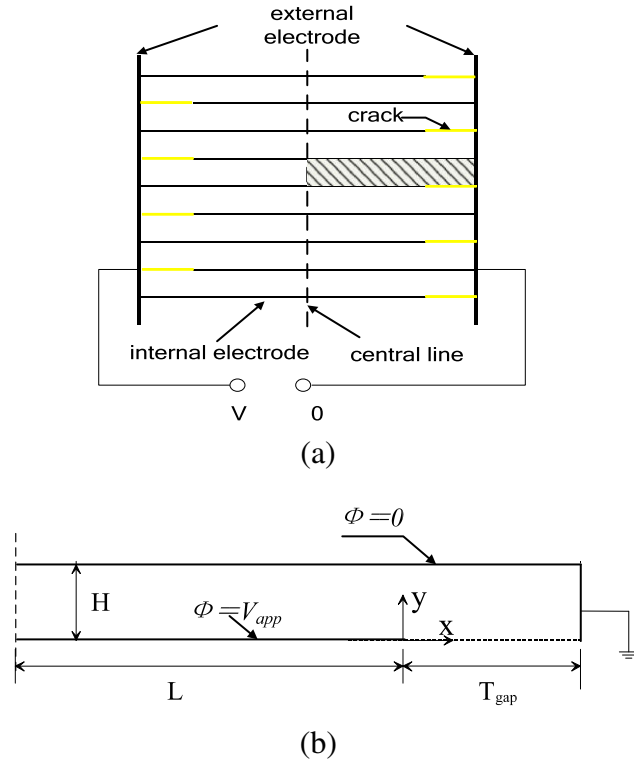


Fig. 9. (a) Schematic of a partially cofired multilayer actuator; (b) schematic of computational model.

At the top electrode ($-L \leq x \leq T_{gap}, y = H$),

$$\phi(x, H) = 0, \quad \tau_{xy} = 0, \quad u_y(x, H) = d_{33}V_{app}. \tag{8d-f}$$

where d_{33} is a piezoelectric constant listed in Table 1. The last equation above is based on the fact that for an integrated actuator, most of the piezoelectric layer covered by electrodes undergoes uniform linear deformation.

At the left boundary of Fig. 9b ($x = -L$),

$$D_x = 0, \quad u_x(-L, y) = 0, \quad \tau_{xy} = 0 \tag{8g-i}$$

Table 1
Material constants of PZT.

Name of parameters (Unit)	Value
Young's module (GPa)	52
Poisson's ratio, ν	0.3
Dielectric permittivity, ϵ^T/ϵ_0	4500
Piezoelectric constants, d_{33} (m/V)	6.40E-10
d_{31} (m/V)	-3.20E-10
d_{15} (m/V)	-3.20E-10
Coercive field, E_c (MV/m)	1.0
Remnant strain e_{11}^R, e_{22}^R	-2.00E-3
Remnant strain e_{33}^R	4.00E-3
Remnant polarization, P^R (C/m ²)	0.25
Spontaneous polarization, P^S (C/m ²)	0.3

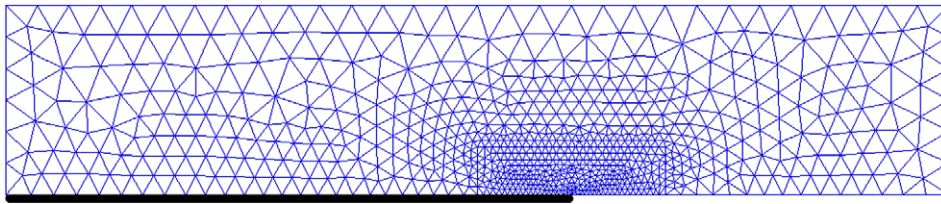


Fig. 10. Finite element mesh.

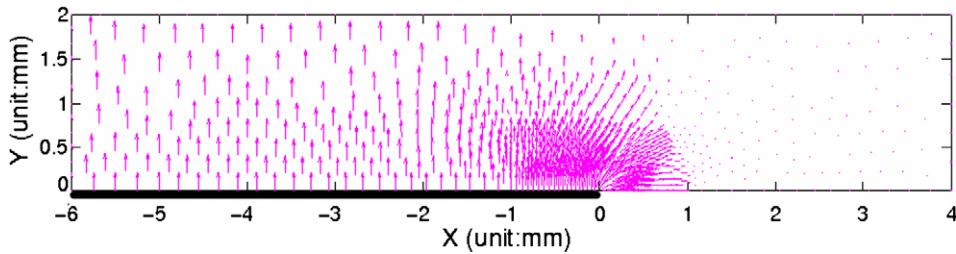


Fig. 11. Distribution of the spontaneous polarization after initial poling in the partially cofired design.

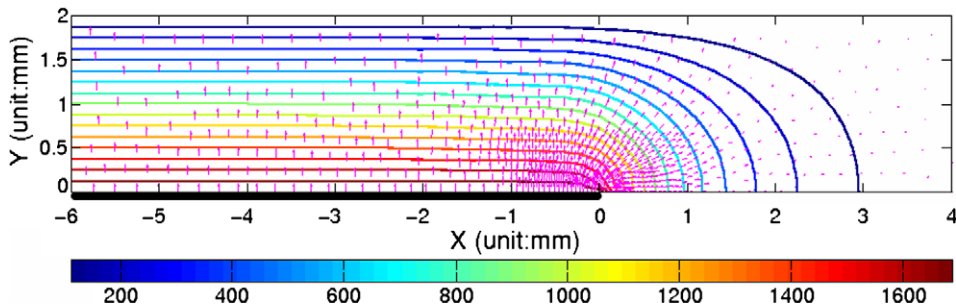


Fig. 12. Electric field vectors and potential contour in the partially cofired design.

At the right electrode ($x = T_{gap}$),

$$\phi(T_{gap}, y) = 0, \quad \sigma_{xx} = 0, \quad \tau_{xy} = 0 \tag{8j-1}$$

At the bottom boundary ahead of electrode tip ($0 \leq x \leq T_{gap}, y = 0$),

$$D_y = 0, \quad \tau_{xy} = 0, \quad \sigma_{yy} = 0 \tag{8m-0}$$

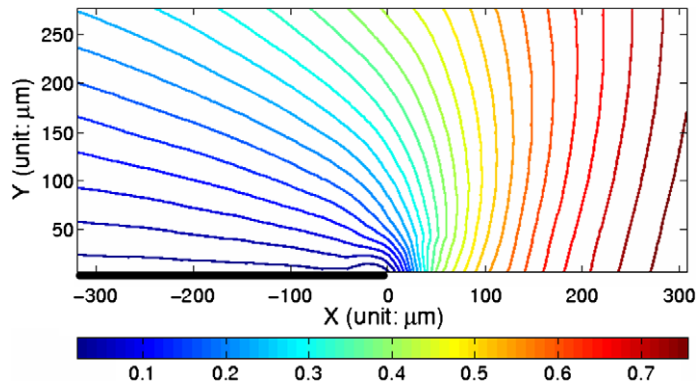


Fig. 13. Numerically determined y-direction displacement field in the partially cofired design (unit: μm).

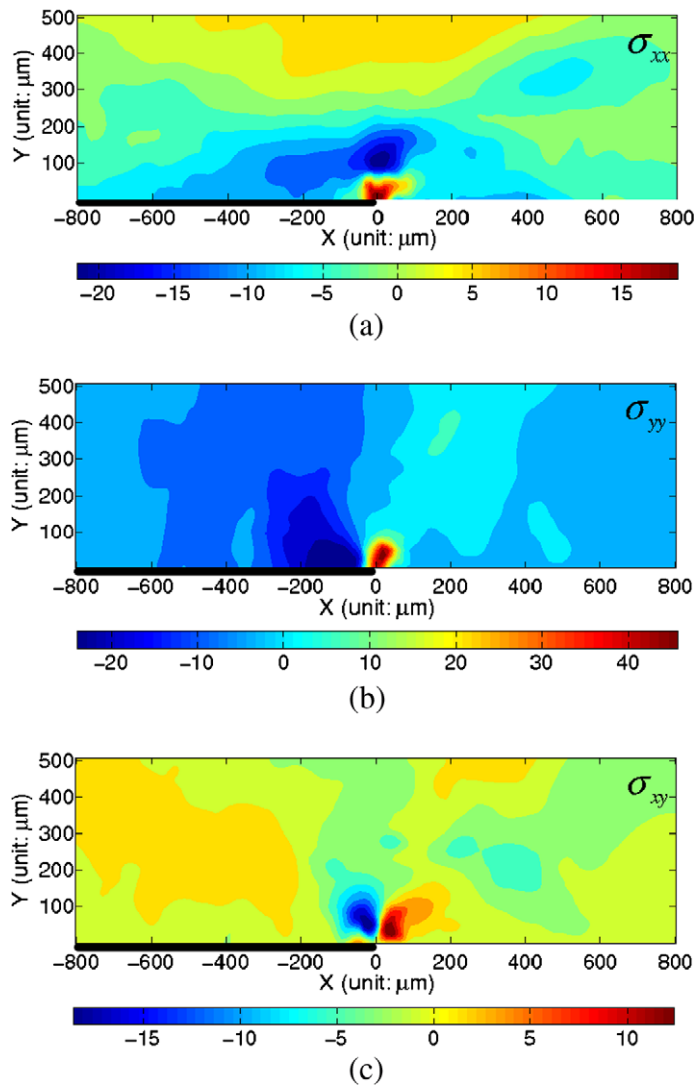


Fig. 14. Calculated stress distributions near the electrode tip in the partially cofired design under $E = 900$ V/mm, unit: MPa. (a) σ_{xx} distribution; (b) σ_{yy} distribution; (c) τ_{xy} distribution.

The triangular elements are used in this simulation, and the mesh is refined near the electrode edge (Fig. 10). Here, the dimension of the computational model is selected as the same as that of experimental specimen. The length of electrode and thickness of the actuator are $L = 6$ mm, $H = 2$ mm, respectively. The length of the interlayer gap is $T_{gap} = 4$ mm. The material constants for an individual domain in the FEM analysis are listed in Table 1, and the corresponding material constants for each element can be computed by volume averaging according to Appendix A.

3.3. Finite element analysis of electroelastic field near the electrode tip of the partially cofired layered actuator

The proposed FEM can simulate the evolution of domain-switching in ferroelectrics. As we know, the unpoled polycrystalline ferroelectric material is not piezoelectric. Therefore, similar to the experimental procedures, the computational model should be firstly polarized under an applied electric field that is sufficiently larger than coercive field E_c such that the domain would switch thoroughly and the polarization would be reoriented along the direction of electric fields. Fig. 11 shows the distribution of spontaneous polarization vectors after this initial poling. We can see that the polarization in the active region (fully covered by electrodes) is uniform and distributes along y -direction except in the area close to electrode tip, but the inactive region (without coverage of electrodes) is even not polarized sufficiently. The similar poling process and mechanical responses for electrode ferroelectric layers have also been studied by Kamlah and Böhle (2001) based on their FE codes.

In the regular working condition of the layered actuator, Fig. 12 shows the distribution of electric field vectors and the contour lines of electric potential for ceramic layer under the electric loading $E = 900$ V/mm. We note that the electric field near the electrode tip is intensely concentrated as expected, which will facilitate domain-switching and stress concentrations in this small region.

To directly compare the displacements from numerical results with experimentally measured data (see Fig. 4), the displacement of pre-poled configuration at zero electric field is recorded as the reference of original displacement, and the same electric loading $E = 900$ V/mm as that in our experiment is adopted. Fig. 13 shows the y -direction displacement from our simulation, and the origin of this coordinate system is also chosen at the electrode tip. The right portion of bottom boundary from 0 to $300 \mu\text{m}$ is an interlayer gap with approximately free surfaces between layers. It is found that both the experimental and numerical results show the obvious deformation concentration near the electrode edge, especially behind the electrode tip. Both the patterns and the magnitude are in good agreement with our experimental results shown in Fig. 4. The results imply that the small region near the electrode edge is intensely strained due to the incompatible deformation, which can result in a highly stress concentration, even the crack initiation and growth, and finally lead to the damage of devices.

As demonstrated above, the accordance between experimental and FEM results sufficiently indicates that the nonlinear FEM embedding domain-switching is an effective tool to simulate the complicated electromechanical behaviors in ferroelectric structures which provides us confidence to further study the concentrated stress field near electrodes, which may play a central role in the failure of devices.

The distributions of stress components σ_{xx} , σ_{yy} and τ_{xy} under the same electric field obtained by the nonlinear FEM are shown in Fig. 14. It should be pointed out that these stresses are total stresses, i.e. the residual stress due to the poling process is also included. We can see that the stress distributes very complexly in the vicinity of the electrode tip, and the stress concentrations are significant. In particular, the vertical stress σ_{yy} is much higher than the other components and can even reach as high as 50 MPa, nearly the magnitude of the strength of piezoelectric ceramics. Therefore, it is believed that the tensile vertical stress σ_{yy} plays a key role in the failure of multilayer actuators, which is consistent with our experimental observation that the delamination occurs on the ceramic–electrode interface (see Fig. 6). However, this stress field concentration is only confined to a small zone near the electrode tip.

4. Comparison of electroelastic fields between partially and fully cofired designs

For most multilayer actuators, the ceramic layers and the alternating internal electrodes are firmly cofired together, i.e. fully cofired as shown in Fig. 2a, so that the whole device can be regarded as a “perfect” integrated bulk without defects and might possess a higher reliability compared to the partially cofired structure including a crack-like gap ahead of electrode tip.

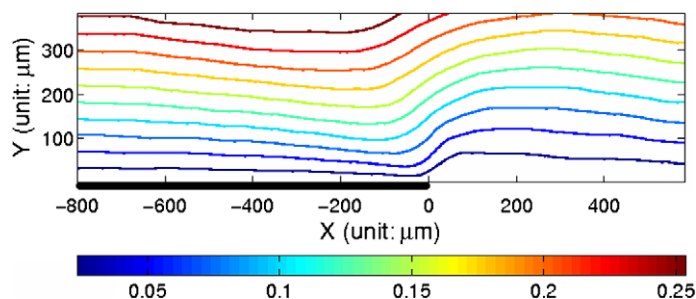


Fig. 15. Numerically determined y -direction displacement field in the fully cofired design (unit: μm).

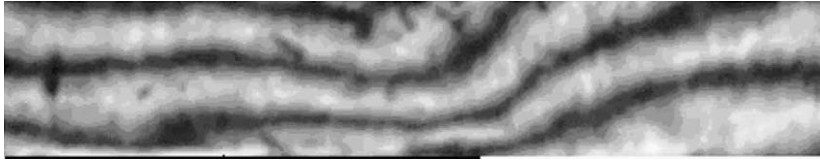


Fig. 16. Experimental y-direction displacement patterns in the fully cofired design from Moiré interferometry (Qiu, 2004).

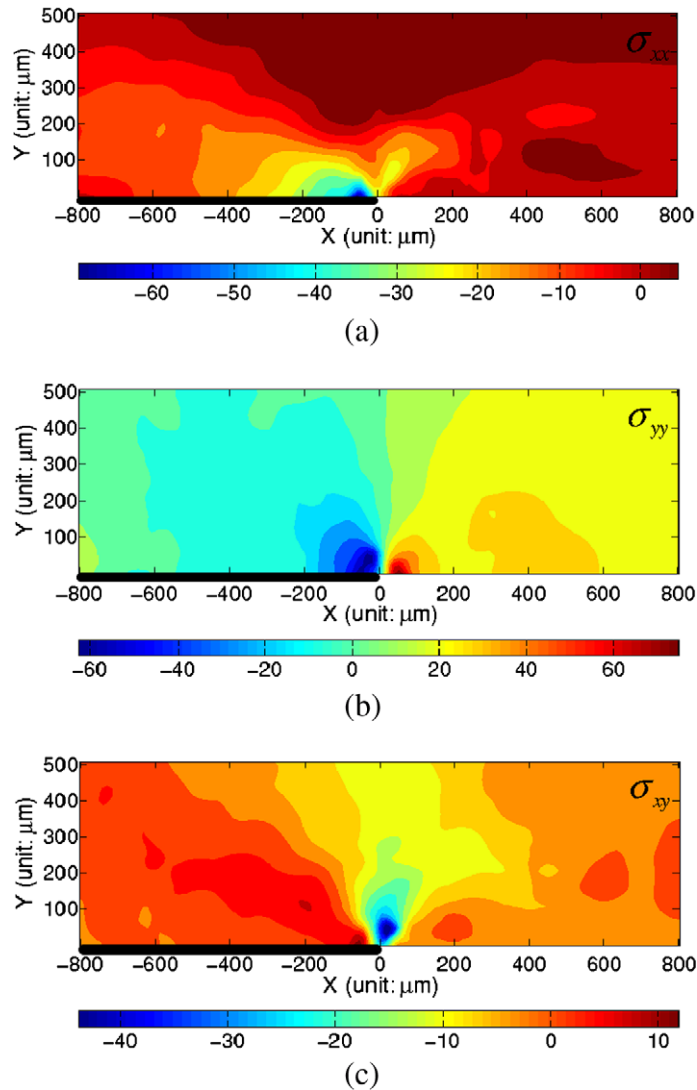


Fig. 17. Calculated stress distributions near the electrode tip in the fully cofired design under $E = 900$ V/mm, unit: MPa. (a) σ_{xx} distribution; (b) σ_{yy} distribution; (c) τ_{xy} distribution.

But can the fully cofired design really improve the reliability of multilayer structures? In the following analysis, this fully cofired model will be studied by our nonlinear FEM as well, and then compared with the previous partially cofired model.

The computational model for fully cofired design can also be selected as Fig. 9b. All boundary conditions are the same except the following y-direction condition on the interlayer gap,

$$v(x, 0) = 0, \quad 0 \leq x \leq T_{gap}, \quad (9)$$

which is used to replace Eq. (80).

This simulation is carried out by the FEM and the contour lines of vertical displacement are shown in Fig. 15, and an experimental deformation field of a fully cofired actuator from morié interferometry (Qiu, 2004) is presented in Fig. 16 to

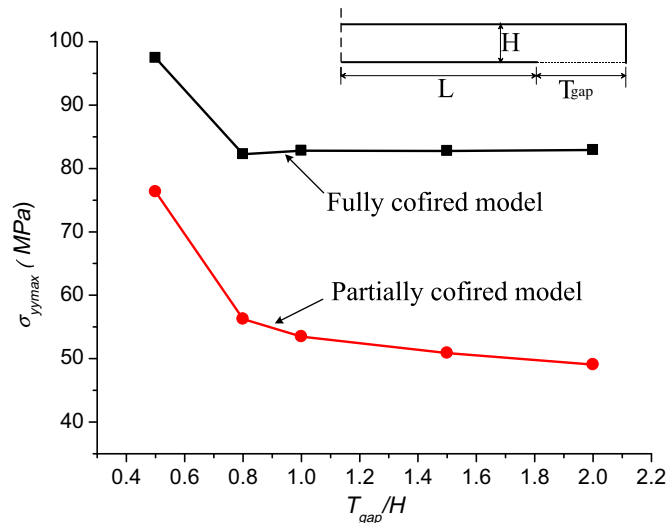


Fig. 18. Maximum normal stresses vs. dimension of electrodes.

compare with the numerical results. Although the dimension and material properties of actuators between the two are different, the patterns of deformation fields from the measurement and simulation are quite similar. This agreement is another validation of our nonlinear FEM codes. It can also be noted that the deformation for fully cofired design totally differs from that of partially cofired design (see Figs. 4 and 15) due to the influence of interlayer gap.

Consequently, the stress components in this case near the electrode tip are presented in Fig. 17. It is noted that the most dangerous stress component is still σ_{yy} , which reaches its maximum positive value in front of the electrode tip and is approximately 50% higher than the corresponding peak value in the partially cofired design. The results show a complete difference from the simple mechanical problem with defects. It should be pointed out that both simulations on fully and partially cofired models are carried out under the same electric loadings and with the same computational meshes for the convenience of comparison. We therefore can draw an interesting conclusion that the crack-like “defects” in the partially cofired layered actuators, i.e. the interlayer gaps, can efficiently reduce the maximum tensile stress level compared to that in “perfect” fully cofired actuators, which implies that the partially cofired design is more reliable than the fully cofired one.

The different stress concentrations in two designs might be understood as follows. In electromechanical structures, the embedded internal electrode can be regarded as an electric flaw that leads to the electric field and stress concentration at its tip. Since the ferroelectrics in layered actuators are not uniformly poled as shown in Fig. 12, the electric field induced deformation is incompatible, especially between the internal electrode-covered active region and the uncovered inactive region. The fully cofired design forcedly makes this incompatible deformation match such that the tensile stress at the interface between layers is higher, whereas the partially cofired design allows the active and inactive regions to deform relatively free, and the stress concentration in the neighborhood of electrode tip can be efficiently released.

5. Geometrical dimension optimization to further relieve stress concentration in piezoelectric layered actuators

One of the objectives in this paper is to find effective ways to relax the stress concentrations in the neighborhood of electrode tip to improve the reliability of devices. Although some new techniques, such as floating electrode method (Maeng et al., 2005), have been developed to decrease the internal stress concentration, they also complicated the manufacturing process at the same time. However, as mentioned above, the partially cofired design is easily manufactured and has a relative low stress concentration compared to the traditional fully cofired design. In this section we will further investigate the influence of the geometrical dimension of the electrode on the stress concentration.

The strain and stress concentration in the neighboring region of electrode tip are induced by the non-uniform electric field, which depends on the non-dimensional ratio T_{gap}/H (see in Fig. 9b), so this ratio is set as the optimal variable here. It should be illustrated that only the length of interlayer gap ahead of electrodes T_{gap} varies and the thickness of layers H keeps constant in our FE analysis. Since the ferroelectric ceramics are much more likely to fracture under the tensile stress compared to compressive stress, and either in the fully or partially cofired model the maximum tensile stress σ_{yy} near the electrode tip is much higher than other stress components and is regarded as the critical damage factor. Therefore, it is reasonable to define the maximum σ_{yy} as the objective function in the optimization.

Fig. 18 shows the variation of the maximum y -direction stress σ_{yy} as a function of the geometrical dimension ratio T_{gap}/H . It can be found that for each geometrical configuration of electrodes, the maximum normal stresses σ_{yy} in fully cofired structures are higher than their counterparts in partially cofired one. Moreover, it is noted from Fig. 18 that, if $T_{gap}/H > 0.8$, both of the curves tend to flatten, which means that the maximum σ_{yy} tends to be less sensitive to this ratio, but there is a significant

increase of the maximum σ_{yy} with the decrease of T_{gap}/H less than 0.8. Therefore, if the horizontal internal electrode is too close to the vertical external electrode, the stress singularity will be more intense, and the facilitation of electric breakdown is another considerable risk due to the high electric field. On the other hand, if the total size of the actuator is fixed, i.e. $2(L + T_{gap})$ keeps constant, a higher generative force for ceramic actuators requires a large effective coverage length of internal electrodes $2L$, or a small T_{gap} . These requirements from both aspects are contradictory. Therefore, to keep the balance among large generative force, resistance of electric breakdown and low concentrated normal stress, the configuration of electrodes at approximately $T_{gap}/H = 1$ is recommended for designing of multilayer actuators.

6. Conclusions

We have studied the electroelastic field concentration around the electrode tip both in partially and fully cofired multilayer actuators via experimental and numerical methods. The following conclusions have been achieved in this paper.

- (i) Under the electric loading, the full displacement field around the electrode tip of layered actuator was accurately measured with high resolution by Digital Speckle Correlation Method (DSCM) and optical microscopy, which shows that the intense deformation occurs near the electrode tip.
- (ii) To accurately account for the domain-switching in ferroelectrics occurring near the electrode tip, a domain-switching embedded nonlinear electromechanical finite element method is developed, in which a new Double Gibbs Free Energy criterion is proposed to simulate the fully coupled electromechanical field and domain evolution in ferroelectric materials. The numerical results of FEM simulation are found in good agreement with the experimental measurements.
- (iii) Two major failure mechanisms of multilayer actuators are found in our experiments, and the failure path induced by electrical breakdown and the delamination between the ceramic layers ahead of electrode edge are observed by using optical microscope. The mechanical fracture path is consistent with the stress analysis of the FEM prediction. It is concluded that the normal stress σ_{yy} , which is much higher than other stress components, is the main cause of mechanical failure.
- (iv) The electromechanical fields near the electrode tip in the fully and partially cofired layered actuators obtained by our nonlinear FEM are compared. An interesting conclusion can be drawn that the crack-like “defects”, i.e. the interlayer gaps, in the partially cofired layered actuators can significantly reduce the maximum tensile stress level compared with that in “perfect” fully cofired actuators, which implies that the partially cofired design is more reliable than the fully cofired one.
- (v) The stress singularity at the electrode tip will be more intense if the internal electrode tip is too close to the external electrode, and the electric breakdown may also take place in this case. By optimizing the geometric dimension, the balance between large generative force, ability of resisting electric breakdown and low concentrated normal stress can be achieved.

Acknowledgement

The authors are grateful for the support by National Natural Science Foundation of China under Grants #10572069, #10121202, #10820101048, #10702034. Support from the Key Grant Project of Chinese Ministry of Education (0306) is also acknowledged.

Appendix A. The relations between elements and domains

In our FEM simulation, 42 representative domains with uniform orientation distribution are chosen for each material point/element to model the behaviors of polycrystalline ferroelectrics. Fig. A1 shows the choosing method for these 42 domains. The sphere in Fig. A1a is an orientation sphere, and each point on the surface represents the domains whose initial spontaneous polarizations are parallel to the vector from the origin to this point. Three Euler angles (θ, ϕ, ψ) defined in Fig. A1b are used to specify the orientation of domains. To construct a uniform orientation distribution, we first introduce a tangent cubic in the sphere as shown in Fig. A1a, so there are 14 specific directions — 8 corners and 6 face centers of the cubic. And for each direction, i.e. for each set of θ and ϕ , three domains have uniformly distributed Euler angle ψ . Each domain has been assigned an integral S as the domain type (from 1 to 6 correspond to six possible orientation choices during the switching process). To obtain the relationships between the element moduli and the domain moduli, we adopt the generalized Reuss assumption that the stress and the electric field are the same for all domains in each element/material point. Therefore, we will rewrite the constitutive equations in term of the stress and electric field as follows. For elements, the constitutive equations become

$$\begin{aligned} \varepsilon_{ij} &= \varepsilon_{ij}^* + M_{ijmn}^E \sigma_{mn} + d_{mij} E_m, \\ D_j &= D_j^* + d_{jmn} \sigma_{mn} + k_{jm}^\sigma E_m, \end{aligned} \quad (\text{A.1})$$

where M_{ijkn}^E , d_{ijk} and k_{ij}^σ are the elastic moduli, piezoelectric moduli and dielectric moduli for element, respectively.

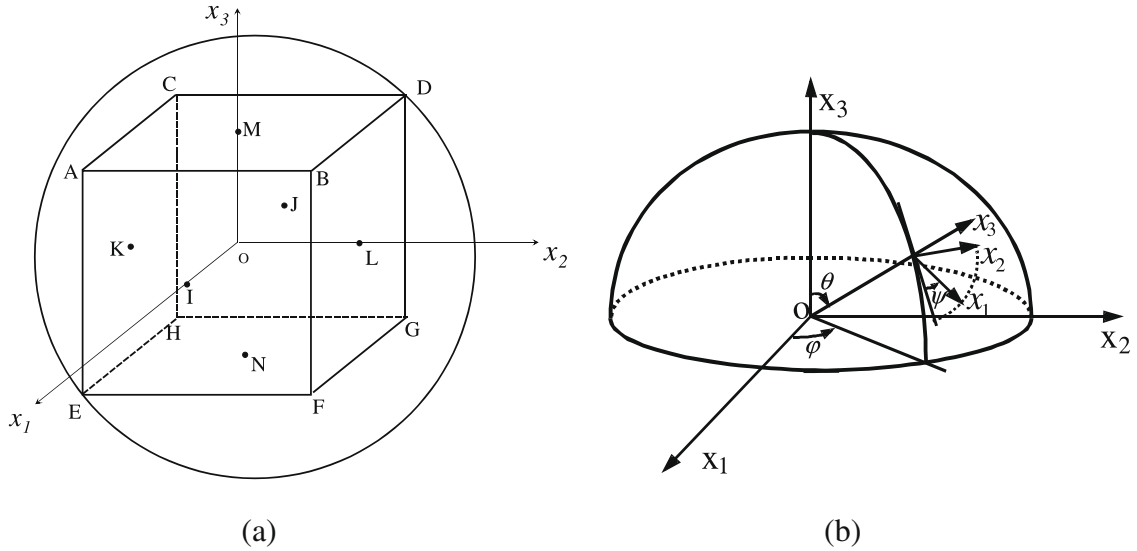


Fig. A1. The choosing method for these 42 domains: (a) orientation sphere; (b) schematic picture of Euler angles.

The constitutive equations of the *l*th domain in the element are

$$\begin{aligned} \epsilon_{ij}^{(l)} &= \epsilon_{ij}^{* (l)} + M_{ijmn}^{E(l)} \sigma_{mn} + d_{mij}^{(l)} E_m \\ D_j^{(l)} &= D_j^{* (l)} + d_{jmn}^{(l)} \sigma_{mn} + k_{jm}^{\sigma(l)} E_m, \end{aligned} \tag{A.2}$$

where $\epsilon_{ij}^{* (l)}$, $D_j^{* (l)}$, $M_{ijmn}^{E(l)}$, $d_{mij}^{(l)}$, $k_{jm}^{\sigma(l)}$ are the remanent strain, remanent electric displacement, elastic moduli, piezoelectric moduli and dielectric moduli of the *l*th domain, respectively, and they are known material constants from Table 1.

Combining (A.1) and (A.2) and generalized Rues assumption yields

$$\begin{aligned} \epsilon_{ij}^* &= \frac{1}{V} \left(\sum_{l=1}^m \epsilon_{ij}^{* (l)} V^{(l)} \right) = \frac{1}{m} \sum_{l=1}^m \epsilon_{ij}^{* (l)}, \quad D_i^* = \frac{1}{m} \sum_{l=1}^m D_i^{* (l)}, \\ M_{ijkn}^E &= \frac{1}{m} \sum_{l=1}^m M_{ijkn}^{E(l)}, \quad d_{ijk} = \frac{1}{m} \sum_{l=1}^m d_{ijk}^{(l)}, \quad k_{ij}^{\sigma} = \frac{1}{m} \sum_{l=1}^m k_{ij}^{\sigma(l)} \end{aligned} \tag{A.3}$$

where *m* is the number of domains in an element, that is 42 in our program. In the derivation, it is assumed that each domain has the same volume fraction. Once we know the domain orientation, we can calculate the macroscopic moduli of elements in Eq. (A.1) at each loading step by averaging over all domains of the local values. Another set of element moduli in Eqs. (5) and (6) can be computed by considering the following relations between moduli,

$$M_{ijmn}^E C_{mkl}^E = I_{ijkl}, \quad e_{mij} = C_{ijkl}^E d_{mkl}, \quad k_{in}^e = k_{in}^{\sigma} - d_{ijk} e_{njik} \tag{A.4}$$

where I_{ijkl} is the fourth order unit tensor.

References

Aburatani, H., Harada, S., Uchino, K., Furuta, A., Fuda, Y., 1994. Destruction mechanisms in ceramic multilayer actuators. *Jpn. J. Appl. Phys.* 33, 3091–3094.
 Chen, W., Lynch, C.S., 1999. Finite element analysis of cracks in ferroelectric ceramic materials. *Eng. Fract. Mech.* 64, 539–562.
 Elhadrouz, M., Ben Zineb, T., Patoor, E., 2006. Finite element analysis of a multilayer piezoelectric actuator taking into account the ferroelectric and ferroelastic behaviors. *Int. J. Eng. Sci.* 44, 996–1006.
 Furuta, A., Uchino, K., 1993. Dynamic observation of crack propagation in piezoelectric multilayer actuators. *J. Am. Ceram. Soc.* 76, 1615–1617.
 Gong, X., Suo, Z., 1996. Reliability of ceramic multilayer actuators: a nonlinear finite element simulation. *J. Mech. Phys. Solids* 44, 751–769.
 Guo, X.H., Fang, D.N., Soh, A.K., Kim, H.C., Lee, J.J., 2006. Analysis of piezoelectric ceramic multilayer actuators based on an electro-mechanical coupled meshless method. *Acta Mech. Sinica.* 22, 34–39.
 Hao, T.H., Gong, X., Suo, Z., 1996. Fracture mechanics for the design of ceramic multilayer actuators. *J. Mech. Phys. Solids* 44, 23–48.
 Hom, C.L., Shankar, N., 1995. A numerical analysis of relaxor ferroelectric multilayered actuators and 2–2 composite arrays. *Smart Mater. Struct.* 4, 305–317.
 Hwang, S.C., Lynch, C.S., McMeeking, R.M., 1995. Ferroelectric/ferroelastic interactions and a polarization switching model. *Acta Metall. Mater.* 43, 2073–2084.
 Hwang, S.C., McMeeking, R.M., 1999. A finite element model of ferroelastic polycrystals. *Int. J. Solids Struct.* 36, 1541–1556.
 Kamlah, M., Böhle, U., 2001. Finite element analysis of piezoceramic components taking into account ferroelectric hysteresis behavior. *Int. J. Solids Struct.* 38, 605–633.
 Kamlah, M., Liskowsky, A.C., McMeeking, R.M., Balke, H., 2005. Finite element simulation of a polycrystalline ferroelectric based on a multidomain single crystal switching model. *Int. J. Solids Struct.* 42, 2949–2964.

- Kamlah, M., Tsakmakis, C., 1999. Phenomenological modeling of non-linear electro-mechanical coupling in ferroelectrics. *Int. J. Solids Struct.* 36, 669–695.
- Li, X.F., Tang, G.T., 2003. Electroelastic analysis of a piezoelectric layer with surface electrode. *Mech. Res. Comm.* 30, 345–351.
- Liu, B., Fang, D.N., Hwang, K.C., 2000. On the effect of remanent polarization on electro-mechanical fields near an elliptic cavity in poled or depolarized piezoelectric ceramics. *Int. J. Fract.* 103, 189–204.
- Liu, B., Fang, D.N., Hwang, K.C., 2002. Electric-field-induced fatigue crack growth in ferroelectric ceramics. *Mater Lett.* 54, 442–446.
- Liu, T., Oates, W.S., Wan, S., Lynch, C.S., 2005. Crack initiation at electrode edges in PZN-4.5%PT single crystals. *J. Intell. Mater. Sys. Struct.* 16, 373–379.
- Liu, T., Webber, K.G., Lynch, C.S., 2008. Finite element analysis with a ferroelectric and ferroelastic material model. *Integr. Ferroelectr.* 101, 164–173.
- Lu, W., Fang, D.N., Hwang, K.C., 1999. Nonlinear electric-mechanical behavior and micromechanics modeling of ferroelectric domain evolution. *Acta Mater.* 47, 2913–2926.
- Maeng, S.Y., Lee, D.K., Choi, J.W., Kim, H.J., Kang, C.Y., Nahm, S., Yoon, S.J., 2005. Design and fabrication of multilayer actuator using floating electrode. *Mater. Chem. Phys.* 90, 405–410.
- McMeeking, R.M., Landis, C.M., 2002. A phenomenological multi-axial constitutive law for switching in polycrystalline ferroelectric ceramics. *Int. J. Eng. Sci.* 40, 1553–1577.
- Narita, F., Yoshida, M., Shindo, Y., 2004. Electroelastic effect induced by electrode embedded at the interface of two piezoelectric half-planes. *Mech. Mater.* 36, 999–1006.
- Peter, W.H., Ranson, W.F., 1982. Digital image technique in experimental stress analysis. *Opt. Eng.* 21, 427–431.
- Qiu, W., Kang, Y.L., Sun, Q.C., Qin, Q.H., Lin, Y., 2004. Stress analysis and geometrical configuration selection for multilayer piezoelectric displacement actuator. *Acta Mech. Solida Sinica* 17, 323–329.
- Qiu, W., 2004. Moiré interferometry experimental technique and image processing method for PZT material. Master Dissertation. Tianjin University, Tianjin.
- Ru, C.Q., 2000. Exact solution for finite electrode layers embedded at the interface of two piezoelectric half-planes. *J. Mech. Phys. Solids* 48, 693–708.
- Sabatè, N., Vogel, D., Gollhardt, A., Keller, J., Michel, B., 2006. Measurement of residual stressed in micromachined structures in a microregion. *Appl. Phys. Lett.* 88, 071910.
- Shindo, Y., Yoshida, M., Narita, F., Horiguchi, K., 2004. Electroelastic field concentrations ahead of electrodes in multilayer piezoelectric actuators: experiment and finite element simulation. *J. Mech. Phys. Solids* 52, 1109–1124.
- Su, Y., Landis, C.M., 2007. Continuum thermodynamics of ferroelectric domain evolution: theory, finite element implementation, and application to domain wall pinning. *J. Mech. Phys. Solids* 55, 280–305.
- Uchino, K., Takahashi, S., 1996. Multilayer ceramic actuators. *Curr. Opin. Solid State Mater. Sci.* 1, 698–705.
- Wang, B.L., Mai, Y.W., 2005. An electrode analysis for multilayer ceramic actuators. *Sens. Act. A* 121, 203–212.
- Winzer, S.R., Shankar, N., Ritter, A.P., 1989. Designing cofired multilayer electrostrictive actuators for reliability. *J. Am. Ceram. Soc.* 72, 2246–2257.
- Xie, H.M., Liu, Z.W., Zhu, H.W., et al., 2004. Study on mechanical behavior of single-wall carbon nanotubes by using digital speckle correlation method. *Opt. Tech.* 30, 449–454.
- Yang, W., Suo, Z., 1994. Cracking in ceramic actuators caused by electrostriction. *J. Mech. Phys. Solids* 42, 649–663.
- Ye, R.Q., He, L.H., 2001. Electric field and stresses concentrations at the edge of parallel electrodes in piezoelectric ceramics. *Int. J. Solids Struct.* 38, 6941–6951.
- Yoshida, M., Narita, F., Shindo, Y., Karaiwa, M., Horiguchi, K., 2003. Electroelastic field concentration by circular electrodes in piezoelectric ceramics. *Smart Mater. Struct.* 12, 972–978.
- Zhang, D.S., Luo, M., Arola, D.D., 2006. Displacement/strain measurements using an optical microscope and digital image correlation. *Opt. Eng.* 45, 033605.